In vivo photoacoustic therapy with cancer-targeted indocyanine green-containing nanoparticles

Aim: The objective of this work was to study the photoacoustic effect of a special nanoparticle for selective cancer cell killing both *in vitro* and *in vivo*. **Materials & methods:** The nanoparticles (NPs) consisting of indocyanine green (ICG), phospholipid–polyethylene glycol (PL–PEG) and folic acid (FA) were used as cancer-targeting nanoprobes. Cancer cells incubated with the ICG–PL–PEG–FA solution were exposed to laser pulses. Finally, tumors in mice were treated with photoacoustic technique. **Results:** High selectivity of the photoacoustic destruction of cancer cells was observed. The tumors in mice after photoacoustic treatment showed a much slower growth rate. **Conclusion:** The destruction of the cells was due to the photoacoustic effect originating from the NPs. The ICG–PL–PEG NP-based photoacoustic therapy would be a safe and highly efficient cancer treatment technique.

Original submitted 21 February 2012; Revised submitted 2 August 2012; Published online 10 September 2012

KEYWORDS: cancer therapy ▪ folic acid ▪ indocyanine green ▪ nanoparticle ▪ near-infrared ▪ phospholipid–polyethylene glycol ▪ photoacoustic therapy ▪ self-assembly

Junping Zhong[1], Sihua Yang[1], Xiaohui Zheng[1], Ting Zhou[1] & Da Xing*[1]

[1]MOE Key Laboratory of Laser Life Science & Institute of Laser Life Science, College of Biophotonics, South China Normal University, Guangzhou 510631, China
**Author for correspondence:*
Tel.: +86 20 8521 0089
Fax: +86 20 8521 6052
xingda@scnu.edu.cn

Nanoparticle (NP)-based technologies with increased site specificity and internalization, such as photoacoustic, photothermal and photodynamic therapies, are considered to be more efficient and less harmful compared with conventional cancer therapeutics [1–9]. Photoacoustic therapy uses the photoacoustic effect of nanoprobes for targeting and selectively destroying cancer cells [10]. It is based on the photoacoustic effect – converting optical energy into acoustic energy. This phenomenon appears when the NPs are exposed to a short-pulsed laser beam. As a consequence, some of the light is absorbed and partly converted to an acoustic wave. This wave is generally called a photoacoustic wave [11–14]. It has been reported that cancer cells can be killed by the strong photoacoustic wave of intracellular single-walled carbon nanotubes under the irradiation of a pulsed laser [7].

The photoacoustic technique has several potential advantages:

- Mechanical mechanism of cell damage without causing toxicity and drug resistance;
- With this approach, the laser power used for cancer killing is reduced 150–1500-times and the therapy efficiency is improved [7];
- The photoacoustic effect can not only be used for cancer therapeutics but also for high-efficiency photoacoustic imaging application.

In the near-infrared (NIR) 700–1100-nm region, human tissue has the lowest absorption coefficient and light can penetrate deepest into biological tissue [15,16]. Combined with NIR probes, photoacoustic therapy is particularly attractive for the destruction of selective cancer cells. Indocyanine green (ICG) is a suitable candidate for developing clinical photoacoustic therapy probes, since it is currently the only US FDA-approved dye that absorbs strongly in the NIR range [17,18]. In addition, ICG exhibits extraordinarily high optical adsorption; it is already used as a contrast agent for photoacoustic imaging [19–21]. According to the parameter of optical absorption divided by weight, ICG is seven-times more efficient than single-walled carbon nanotubes and approximately 8500-times more efficient than commercial gold nanorods, with a peak absorption at 780 nm [22].

The authors developed a NP (ICG–phospholipid–polyethylene glycol [PL–PEG]) consisting of ICG and PL–PEG as a photoacoustic therapy probe [23]. These NPs have overcome numerous limitations of ICG, such as poor aqueous stability, concentration-dependent aggregation and lack of target specificity [24–27]. The NPs provide multiple advantages:

- The NPs are biocompatible and relatively nontoxic;
- The NPs can improve the molecular stability of ICG and prolong its plasma half-life;

Future Medicine part of fsg

- The size of the NPs (~18 nm) allows extravasation and permeation into tumor tissue. They are also small enough to avoid clearance by the reticuloendothelial system [28–31];
- The hydrophilic PEG surrounding the NP surface renders the NPs sterically stable, protecting them from mononuclear phagocytic system uptake and therefore increasing the drug circulation time.

In addition, these NPs have been evaluated for stability under biological environments and demonstrated to be suitable for photothermal therapy in the authors' previous work [23].

In this article, the properties of ICG–PL–PEG NPs were examined, including morphology, absorption and fluorescence spectra. The photoacoustic effect of the NPs was also investigated. To confirm the destructive power of the ICG–PL–PEG NP's explosion, the photoacoustic effect of these NPs was evaluated *in vitro* using a cell-like hydrogel model. By functionalizing with folic acid (FA), the probe (ICG–PL–PEG–FA) can selectively enter into cancer cells that overexpress the folate receptor (FR) at the cell membrance. The target specificity of these NPs was evaluated *in vitro* via fluorescent microscopy. At first, the targeting ICG–PL–PEG–FA NPs conjugate to the FRs at the cellular membrane, leading to a relatively high surface concentration of the ICG–PL–PEG–FA NPs. Later, the targeting NPs were endocytosed by the cell. Photoacoustic therapy with the targeting ICG–PL–PEG–FA NPs for killing cancer cells was then carried out *in vitro*. Tumor targeting and *in vivo* distribution of ICG–PL–PEG–FA were investigated. Finally, the highly efficient destruction of solid tumors *in vivo* by cancer-targeting photoacoustic therapy was confirmed. During photoacoustic treatment, the temperature changes were monitored by an infrared thermal camera. The temperature increased by no more than 3°C. Therefore, the destructive effect of ICG–PL–PEG–FA on cancer cells can be considered to be mainly mechanical damage induced by the strong shockwave rather than thermal damage caused by high temperatures.

Materials & methods

Materials

1,2-distearoyl-*sn*-glycero-3-phosphoethanolamine-*N*-[amino/carboxy(PEG)2000] was obtained from Avanti Polar Lipids Inc. (AL, USA). ICG for injection was purchased from Dan Dong Yi Chuang Company (Dandong, Liaoning, China). Cell-counting kit 8 was obtained from Dojindo Laboratories (Kumamoto, Japan). FA, *N*-hydroxysulfosuccinimide and 1-ethyl-3-(3-dimethylaminopropyl)carbodiimide were obtained from Sigma-Aldrich Corporation (MO, USA). FR, FL-257, polyclonal antibody (Santa Cruz, CA, USA) and other chemicals used in this work were all of analytical grade. All of the reagents were used without further purification.

Preparation of ICG–PL–PEG NPs

Preparation of ICG–PL–PEG NPs and the targeting ICG–PL–PEG–FA NPs was performed following the procedures according to Zheng *et al.* [23].

Characterization experiments

The absorption spectra of ICG solution and plain ICG–PL–PEG NPs were investigated by a UV/vis spectrometer (Lambda 35, Perkin-Elmer, MA, USA). Fluorescence spectra were investigated by an LS-55 fluorescence spectrophotometer (Perkin-Elmer) with an excitation of 780 nm.

A JEM-100CXII (Jeol Inc., Tokyo, Japan) transmission electron microscope with parameters of 100 kV voltage and 70 pA current was used to examine the morphology and size of the probe. The distribution of diameters was determined by using transmission electron microscopy images of at least 100 NPs.

Photoacoustic signal of ICG–PL–PEG NPs

A custom-made photoacoustic imaging system was used to test the photoacoustic effect of the NP solutions. As illustrated in Figure 1A, a 0.8-mm diameter silicon tube was fixed in a glass water tank. A total of 10 ml of ICG–PL–PEG NPs with ICG concentrations of 10, 20, 40 and 80 μg/ml were injected into the tube to determine their photoacoustic signals. An optical parametric oscillator (OPO; Vibrant 532 I, Opotek, CA, USA) was used for light illumination. The OPO operated at 808 nm with a pulse duration of 10 ns and a pulse repetition rate of 10 Hz was used to irradiate the samples for generating photoacoustic signals. An ultrasound transducer with 75 MHz center frequency and 65% fractional bandwidth was used to receive the photoacoustic signals.

Preparation of a cell-like model

Alginate–polylysine–alginate microcapsules containing ICG–PL–PEG NPs were prepared

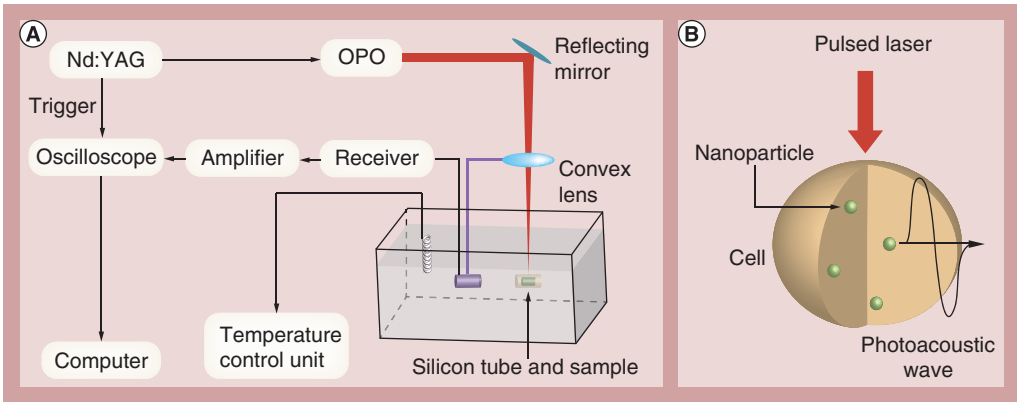

Figure 1. Photoacoustic system and representation of the photoacoustic therapy. (A) The photoacoustic system. **(B)** Cancer cell-targeting photoacoustic therapy.
Nd:YAG: Neodymium-doped yttrium aluminum garnet; OPO: Optical parametric oscillator.

using a water-in-oil-in-water double emulsion method. A 5-ml aqueous solution containing sodium alginate (1.5% w/w) and ICG–PL–PEG NPs (containing 1 mg/ml ICG) was briefly dispersed in an isooctane solution containing a lipophilic surfactant (Span 85, 2.0% w/w) by using a mechanical stirrer at 8000 rpm. After 15 min, 15 ml of 5 M $CaCl_2$ solution was added to form Ca–alginate microspheres. The formed emulsion was left stirring for 1 h. The microspheres were collected by filtration and washed three times with deionized water. Ca–alginate beads were suspended in a solution of polylysine (0.1% w/w) for 10 min, washed with deionized water and then immersed in alginate solution (0.05% w/w) for 10 min. The resulting microcapsules containing ICG–PL–PEG NPs were washed with deionized water and stored at 4°C for further experiments [7].

Cell culture & transfection

Mouse mammary tumor line EMT6 cells were cultured in Roswell Park Memorial Institute medium 1640 (GIBCO, NY, USA) supplemented with 15% fetal bovine serum, penicillin (100 units/ml) and streptomycin (100 µg/ml) in 5% CO_2/95% air at 37°C in a humidified incubator. FR^+ EMT6 cells were obtained by culturing the EMT6 cells in FA-free medium. It is known that the FA-starved cells overexpress FRs on the cell surfaces. EMT6 cells were passaged for at least four times in the FA-free medium before use to ensure that all FRs were available on the surface of the cells. FR^- cells were obtained by culturing cells in medium with abundant FA to give few available free FRs on the cell surfaces. These procedures ensured a very high level of available FRs on the FR^+ cells and a very low level of available FRs on the FR cells [23].

Confocal laser scanning microscopy

Cells (1×10^4 per well) growing in 35-mm Petri dishes were incubated with the ICG–PL–PEG–FA solution (containing 10 µg/ml ICG, mass ratio ICG:PL–PEG = 1:100) for 1 h at 37°C. FR^+ cells were rinsed with phosphate-buffered saline (PBS) three times and replaced with fresh FA-free medium. FR^- cells were also rinsed with PBS three times and replaced with the medium with abundant FA. The cells were observed by a commercial laser scanning microscope combination system (LSM510/ConfoCor2, Zeiss, Jena, Germany) equipped with a Plan-Neofluar 40 /1.3 numerical aperture oil differential interference contrast objective. The ICG–PL–PEG–FA NPs were excited at 633 nm with a He–Ne laser, and emitted light was recorded through a long-pass 650-nm filter.

Flow cytometry analysis

In the authors' experiments, cells were cultured in six-well dishes (1×10^6 per well). FR^+ EMT6 cells were cultured in FA-free medium to ensure that all FRs were available on the surface of the cells. FR^- cells were cultured in medium with abundant FA to reduce the available free FRs on the cell surfaces. Cells were then harvested and fixed with 4% paraformaldehyde in PBS for 10 min at 37°C. Fixed cells were blocked in PBS solution containing 1% bovine serum albumin for 10 min at room temperature and then incubated with FL-257 polyclonal antibody (1:50) at room temperature for 60 min, before being incubated with fluorescein-conjugated Affinipure goat anti-rabbit IgG (1:50; Proteintech Group, CA, USA) for 30 min in the dark. After washing, the samples were analyzed by flow cytometry (FACScan™, Becton Dickinson, CA, USA). The fluorescence histogram of cells in different treatments was obtained from 10,000 cells.

Selective killing of cancer cells during NIR irradiation

Cancer cells (1×10^4 per well) growing in 35-mm Petri dishes were incubated with the ICG–PL–PEG–FA solution (containing 10 μg/ml ICG at 37°C) for 2 h. FR^+ cells were rinsed with PBS three times and replaced with fresh FA-free medium. FR^- cells were also rinsed with PBS three times and replaced with the medium with abundant FA. The cells were exposed to 808 nm laser pulses (20 mJ/cm^2) for 20 s. After treatment, the cells were observed by a commercial laser scanning microscope combination system (LSM510/ConfoCor 2) equipped with a Plan-Neofluar 40/1.3 numerical aperture oil differential interference contrast objective. The ICG–PL–PEG–FA NPs were excited at 633 nm with a He–Ne laser and the emitted light was recorded through a long-pass 650-nm filter.

Photoacoustic therapy

An OPO operated at 808 nm with a pulse duration of 10 ns and a pulse repetition rate of 10 Hz was used to irradiate the targets. The experiment was conducted with an energy density of 5–25 mJ/cm^2.

Determination of cell cytotoxicity

Cancer cells growing in a 96-well microplate (5×10^3 per well, 100 μl) were incubated with the targeting probe solution (containing 10 μg/ml ICG at 37°C) for 2 h, and then rinsed with PBS three times, followed by irradiation with 808-nm laser pulses (from 5 to 25 mJ/cm^2) for 20 s. Cell cytotoxicity was assessed 12 h after the laser irradiation with CCK-8. The absorbance value at 450 nm (OD450) was read with a 96-well plate reader (Infinite® M200, Tecan, Switzerland) to determine the viability of the cells.

Tumor model

To generate the EMT6 murine breast tumor model, FR^+ EMT6 cells (2×10^6) in a 100 μl solution were subcutaneously injected onto the back of each female Balb/c mouse. The mice were used on days 5–7 after the inoculation of cells, when the tumor volumes approached approximately 100 mm^3.

In vivo biodistribution of ICG, ICG–PL–PEG & ICG–PL–PEG–FA

Biodistribution studies of ICG, ICG–PL–PEG and ICG–PL–PEG–FA were performed as previously reported [32]. Twelve tumor-bearing mice were randomly divided into four groups (n = 3 per group). Mice in group 1 were intravenously injected via the tail vein with 100 μl PBS as a control. Mice in groups 2, 3 and 4 were intravenously injected with 100 μl of ICG, ICG–PL–PEG and ICG–PL–PEG–FA, respectively (all containing 0.1 mg/ml ICG). Whole-body NIR fluorescent images of the mice were taken 6 h after intravenous injection using the Odyssey® Infrared Imaging System (LI-COR, Inc., NE, USA) through an 800-nm channel. The tumors and organs of interest (heart, spleen, lungs, liver and kidneys) were retained for imaging and semiquantitative biodistribution analysis.

Photoacoustic therapy of murine tumors

For *in situ* intratumoral injection photoacoustic tumor treatment, 30 tumor-bearing mice were randomly divided into six groups (n = 5 per group). Mice in groups 1, 2 and 3 were intratumorally injected with 25 μl of ICG, ICG–PL–PEG and ICG–PL–PEG–FA, respectively (all containing 2 mg/ml ICG). At 2 h postinjection, the tumors were treated with the laser. The same amount of ICG–PL–PEG–FA NPs as used in group 3 were injected into group 4 mice, but group 4 did not receive laser treatment. Mice in group 5 were treated with the laser alone, while the last group of mice did not have any treatment.

For the intravenous injection experiment, solutions of ICG, ICG–PL–PEG and ICG–PL–PEG–FA (100 μl, all containing 5 mg/ml ICG) were intravenously injected via the tail vein. After 6 h, the tumors on each mouse in the different groups (n = 5 per group) were treated with the laser. The mice in the control group were intravenously injected with 100 μl PBS.

An OPO laser was used to irradiate tumors for 10 min (1-min interval after each minute of irradiation, 20 mJ/cm^2). The spot size of the laser beam was adjusted to cover the entire tumor.

After treatment, the tumor sizes were measured by a caliper every 2 days and calculated as:

$$Volume\ (V) = tumor\ length \times \frac{tumor\ width^2}{2}$$

Relative tumor volumes were calculated as V/V_0 (V_0 was the tumor volume when the treatment was initiated).

Histology examination

For histological analysis, tumors (n = 3 per group) from the control and treated mice were harvested 3 h after treatment. The major organs of mice were harvested 20 days after treatment, fixed in 10% neutral-buffered formalin,

processed routinely into paraffin, sectioned into 5-µm-thick slices, stained with hematoxylin and eosin (H+E) and examined by light microscopy.

Temperature measurements during NIR radiation

For *in vitro* experiments, the temperature was measured in 3-s intervals with an infrared thermal camera (TVS200EX, NEC, Tokyo, Japan). For *in vivo* measurements, the surface temperatures of the tumors were measured in 30-s intervals with an infrared thermal camera. All of the experiments were conducted at room temperature.

Statistical analysis

Each experiment was performed at least three times. Tests for significant differences between the groups were carried out using the student's *t*-test (two-tailed). Data are presented as the arithmetic mean ± standard error of the mean. Otherwise, representative data are shown.

Results

Characterization of the ICG–PL–PEG probe

Figure 2A is the schematic procedure for production of the ICG–PL–PEG NPs. The PEG-coated, amine-functionalized base nanoprobe (ICG–PL–PEG) is designed to utilize the noncovalent self-assembly chemistry between ICG and PL–PEG. Figure 2B & C show the absorption and fluorescence of freely dissolved ICG and ICG–PL–PEG solution. The concentration of the freely dissolved ICG solution was 5 µg/ml. In the ICG–PL–PEG solution, the concentration of ICG was also 5 µgNml. Both solutions at this concentration showed no quenching effect of the dye. The maximum absorption and emission spectra for freely dissolved ICG are 785 and 808 nm, respectively. The main peaks of the absorption and emission spectra of ICG–PL–PEG shift approximately 20 and 15 nm toward the higher wavelengths compared with freely dissolved ICG (Figure 2B). A transmission electron microscopy image of the ICG–PL–PEG NPs showed that the NPs were spherical and well dispersed, with a core size of approximately 18 nm. The photoacoustic signal generated by ICG–PL–PEG NPs at various ICG concentrations was detected using a pulsed laser as the irradiation source. The choice of laser wavelength was based on the absorbance spectra of ICG–PL–PEG NPs. The photoacoustic signals generated by the ICG–PL–PEG NP solutions are summarized in Figure 2D. The intensity of the photoacoustic signal produced by ICG–PL–PEG was observed to be linearly dependent on the ICG concentrations (R^2 = 0.991; Figure 2E).

Photoacoustic effect of ICG–PL–PEG NPs

To investigate the destructive power of the photoacoustic wave, the ICG–PL–PEG NPs were enwrapped within a type of alginate–polylysine–alginate microcapsule to develop a cell-like hydrogel model (Figure 3A). The microcapsules were approximately 20 µm in size and the thickness of the shell was 1–2 µm. The concentration of ICG in microcapsules was approximately 0.5 mg/ml. With laser treatment (20 mJ/cm^2) for 20 s, ICG–PL–PEG NPs in the microcapsules exploded and broke the microcapsules (Figure 3B).

Selective imaging of cancer cells with the ICG–PL–PEG–FA probe

As the fluorescence intensity shows (Figure 4), in the FR$^+$ cell with excessive FRs, the fluorescence intensity was much higher than that in the FR$^-$ cells with few receptors on the surface.

The uptake of the ICG–PL–PEG–FA NPs into FR$^+$ cells with all available FRs on the cell surface was indicated by fluorescence emission from the EMT6 cells using fluorescence microscopy. The fluorescence emission from just the surface of FR$^+$ cell membranes after incubating with the ICG–PL–PEG–FA NPs for 1 h shows the NPs initially bonded on the cell membrane (Figure 5A). The strong fluorescence of ICG was observed in the cytoplasm after incubation for 3 h (Figure 5B). The results reveal that the NPs had been in the cells. The fluorescence of ICG inside cells obviously decreased after 6 h (Figure 5C). This phenomenon indicates that a large number of NPs discharged out of the cells. All confocal images illustrated that the ICG–PL–PEG–FA NPs did not translocate into the nucleus, as little fluorescence of ICG was observed inside the nucleus. In order to confirm the target specificity, the FR$^-$ cells with few available FRs were used as a control. Little fluorescence was observed in these cells (Figure 5D). The results show that, in the FR$^+$ cells with excessive FRs, the fluorescence intensity of ICG was much higher than that in the FR$^-$ cells with few FRs. The selective uptake of ICG–PL–PEG–FA inside FR$^+$ cells clearly indicates that receptor-mediated endocytosis is more selective and efficient than nonspecific endocytosis.

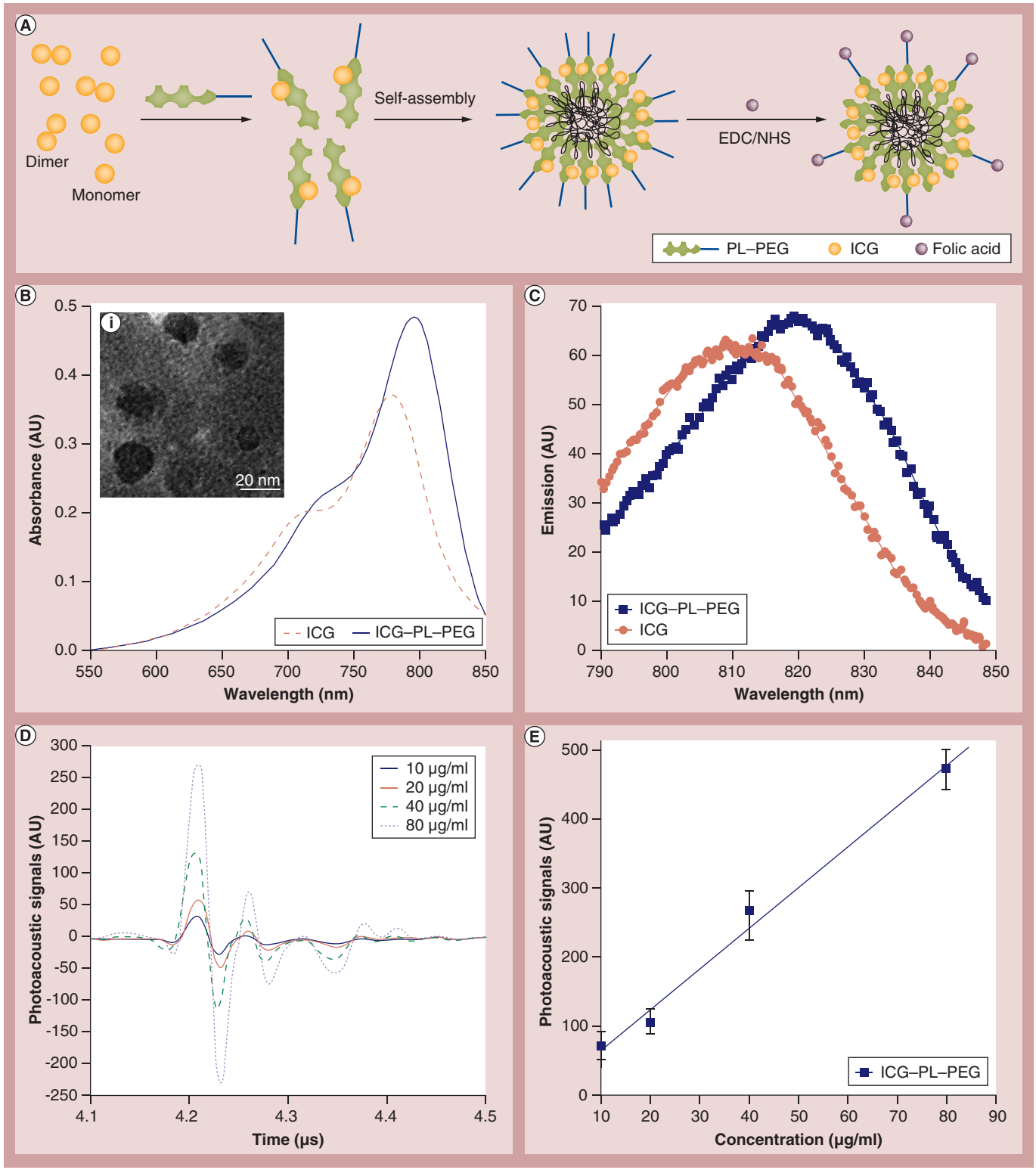

Figure 2. Characterization of indocyanine green–phospholipid–polyethylene glycol nanoparticles. (A) Self-assembly process of ICG-containing nanoparticles (ICG–PL–PEG NPs) and targeted modification of ICG–PL–PEG NPs. Folic acid was linked on the surface via an amidation reaction. **(B)** Absorption spectra of ICG and ICG–PL–PEG NPs, respectively. Peak absorption of ICG–PL–PEG NPs was in the near-infrared region. **(Bi)** A typical transmission electron microscopy image of the ICG–PL–PEG NPs. **(C)** Fluorescence spectra of ICG and ICG–PL–PEG NPs. **(D)** Photoacoustic signals of ICG–PL–PEG NPs at various concentrations. **(E)** The photoacoustic signal produced by ICG–PL–PEG NPs is linearly dependent on the concentrations.
EDC: 1-ethyl-3-(3-dimethylaminopropyl)carbodiimide; ICG: Indocyanine green; NHS: *N*-hydroxysulfosuccinimide; PL–PEG: Phospholipid–polyethylene glycol.
Adapted with permission from [23] © American Chemical Society (2011).

Selective killing of cancer cells using the photoacoustic effect of ICG–PL–PEG–FA NPs

To investigate the photoacoustic effect on cancer cells, FR^+ cells were incubated with the ICG–PL–PEG–FA solution (containing 10 μg/ml ICG) for 2 h. After being washed with PBS, the FR^+ cells were exposed to laser pulses (20 mJ/cm^2) for 20 s. Before laser treatment, the fluorescence in the cytoplasm was strong, but there was no fluorescence in the nucleus, indicating that the NPs were located in cytoplasm (Figure 6Ai). The dividing line between the nucleus and cytoplasm is clear. As shown in the confocal images (Figure 6Aii), drastic cell morphology changes were observed after photoacoustic treatment. The dividing line between the nucleus and cytoplasm became unclear and fluorescence was then observed inside the whole cells. These phenomenons are related to the destruction of cells with photoacoustic therapy. As a comparision, FR^- cells with few available FRs on the surface of the cell membrane were employed as a control. FR^- cells were incubated with the ICG–PL–PEG–FA solution (containing 10 μg/ml ICG) for 2 h. After being washed by PBS, the FR^- cells were exposed to laser pulses (20 mJ/cm^2) for 20 s. The cells remained intact after laser irradiation (Figure 6Aiii). No apparent change of the cellular morphology was observed under these treatments.

To investigate the photoacoustic effect of the cells, the authors monitored the proliferation ratio of cancer cells after laser treatment with ICG and ICG–PL–PEG–FA NPs (with ICG concentrations from 1 to 20 μg/ml). All of the cells were irradiated by laser pulses (20 mJ/cm^2) for 20 s. Cell cytotoxicity was assessed 12 h after laser treatment with CCK-8. As shown in Figure 6B, cell viability of FR^+ cells markedly decreased as the concentration of the ICG–PL–PEG–FA increased, while the FR^- cells retained a survival rate of 95% when treated by laser and ICG–PL–PEG–FA. Furthermore, the death rate of FR^+ cells treated by laser and ICG–PL–PEG–FA was significantly higher than those treated by laser and ICG with the same ICG concentration.

To study the photoacoustic toxicity, FR^+ cells were irradiated by laser with an energy of 5–25 mJ/cm^2 for 20 s. In all of these cases, no significantly negative effect on cell proliferation was observed with irradiation alone. This indicates no obvious cellular toxicity of laser treatment at such a short time. Figure 6C shows that cell lethality increased significantly under laser irradiation in the presence of the probe. Cell viability decreased by 74.6% after laser irradiation (20 mJ/cm^2) in FR^+ cells treated with ICG–PL–PEG–FA NPs (Figure 6C).

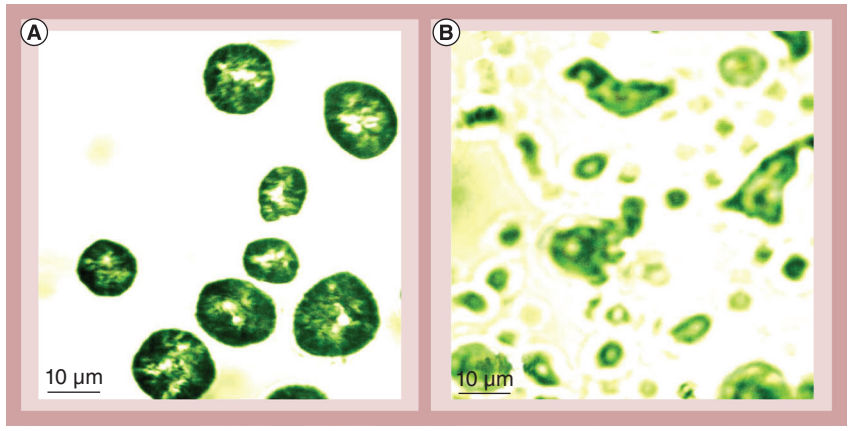

Figure 3. Destructive power of indocyanine green–phospholipid–polyethylene glycol nanoparticles in cell-like microcapsules. (A) Initial cell-like microcapsules with indocyanine green–phospholipid–polyethylene glycol inside. **(B)** The broken microcapsules after laser treatment.

Photoacoustic treatment of tumors through intratumoral injection of different solutions

After validation by *in vitro* experiments, the authors then attempted photoacoustic treatment through intratumoral injection. As is shown in Figure 7B, significant suppression of tumor growth was observed after tumors were injected with the ICG–PL–PEG or ICG–PL–PEG–FA particles and irradiated with the laser pulses, but not with ICG–PL–PEG–FA or radiation alone. All

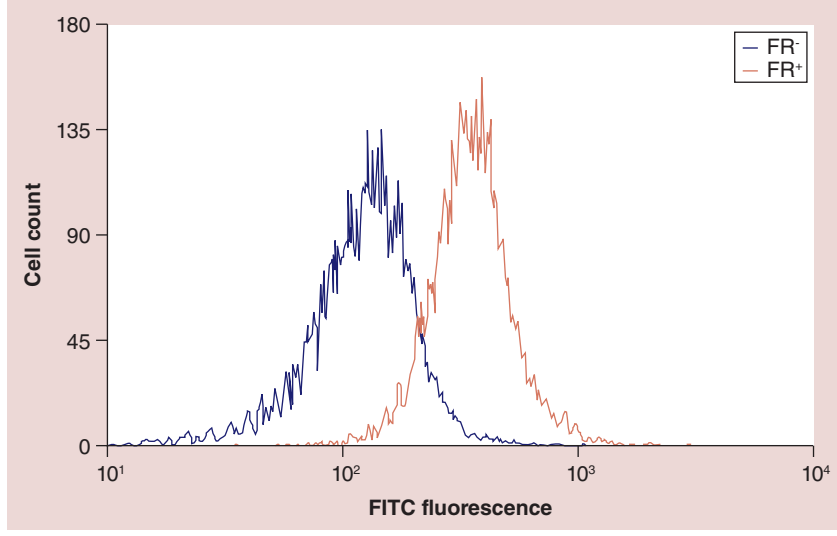

Figure 4. Fluorescence-activated cell-sorting analysis of available folate receptors on the cell surface of folate receptor-positive and -negative cells. For the FR^+ cells with excessive FRs, the fluorescence intensity was much higher than that in the FR^- cells with few FRs on the cell surface.
FITC: Fluorescein isothiocyanate; FR: Folate receptor.

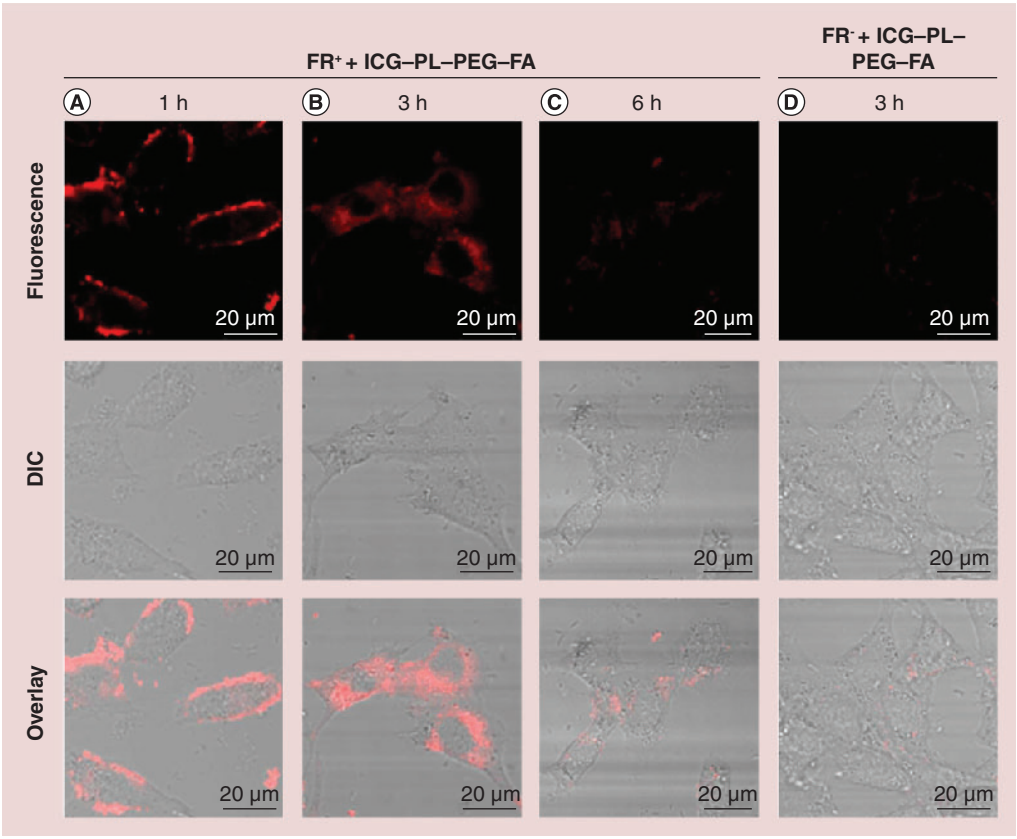

Figure 5. Confocal images of folate receptor-positive and -negative cells after incubation with the indocyanine green–phospholipid–polyethylene glycol–folic acid nanoparticles. (A–C) The fluorescence shows a high uptake level of the ICG–PL–PEG–FA nanoparticles into FR^+ cells. **(D)** Little fluorescence inside cells shows low uptake levels of ICG–PL–PEG–FA nanoparticles into FR^- cells.
DIC: Differential interference contrast measurement; FA: Folic acid; FR: Folate receptor; ICG: Indocyanine green; PL–PEG: Phospholipid–polyethylene glycol.

of the tumors on mice after being injected with the ICG–PL–PEG–FA and exposed to the laser pulses were partially damaged and showed a much slower growth rate.

H+E staining of tumor slices collected from laser- and ICG–PL–PEG–FA-treated mice showed that most tumor cells were severely destroyed (Figure 7Cii), while there was no obvious damage observed in the control tumor slices (Figure 7Ci). These results further confirmed the successful destruction of cancer cells by the photoacoustic treatment.

In vivo biodistribution of ICG, ICG–PL–PEG & ICG–PL–PEG–FA

A whole-animal NIR imaging approach was used to investigate the tumor targeting and *in vivo* distribution of ICG, ICG–PL–PEG and ICG–PL–PEG–FA in nude mice. Figure 8A & B showed that ICG and ICG–PL–PEG were mainly located in the liver, while ICG–PL–PEG–FA had a high accumulation in both the tumor and liver. The mice were sacrificed, and various organs and tissues were collected for imaging analysis. The averaged ICG fluorescent intensity of each imaged organ (after removing the tissue autofluorescence and subtracting the background) was calculated for a semiquantitative biodistribution analysis. The highest fluorescence signal was observed in the tumor for ICG–PL–PEG–FA, suggesting a high accumulation of ICG–PL–PEG–FA in the tumor (Figure 8C).

Photoacoustic treatment of tumors through intravenous injection of different solutions

Motivated by the tumor accumulation of ICG–PL–PEG–FA and its strong NIR optical absorption ability at 808 nm, the authors carried out further *in vivo* intravenous injection photoacoustic treatment. Figure 9A shows that laser and ICG–PL–PEG–FA treatment caused significant tumor suppression. Photoacoustic damage to tumor cells was confirmed by H+E staining. High scathe level was only observed in the group with laser treatment plus ICG–PL–PEG–FA injection (Figure 9B).

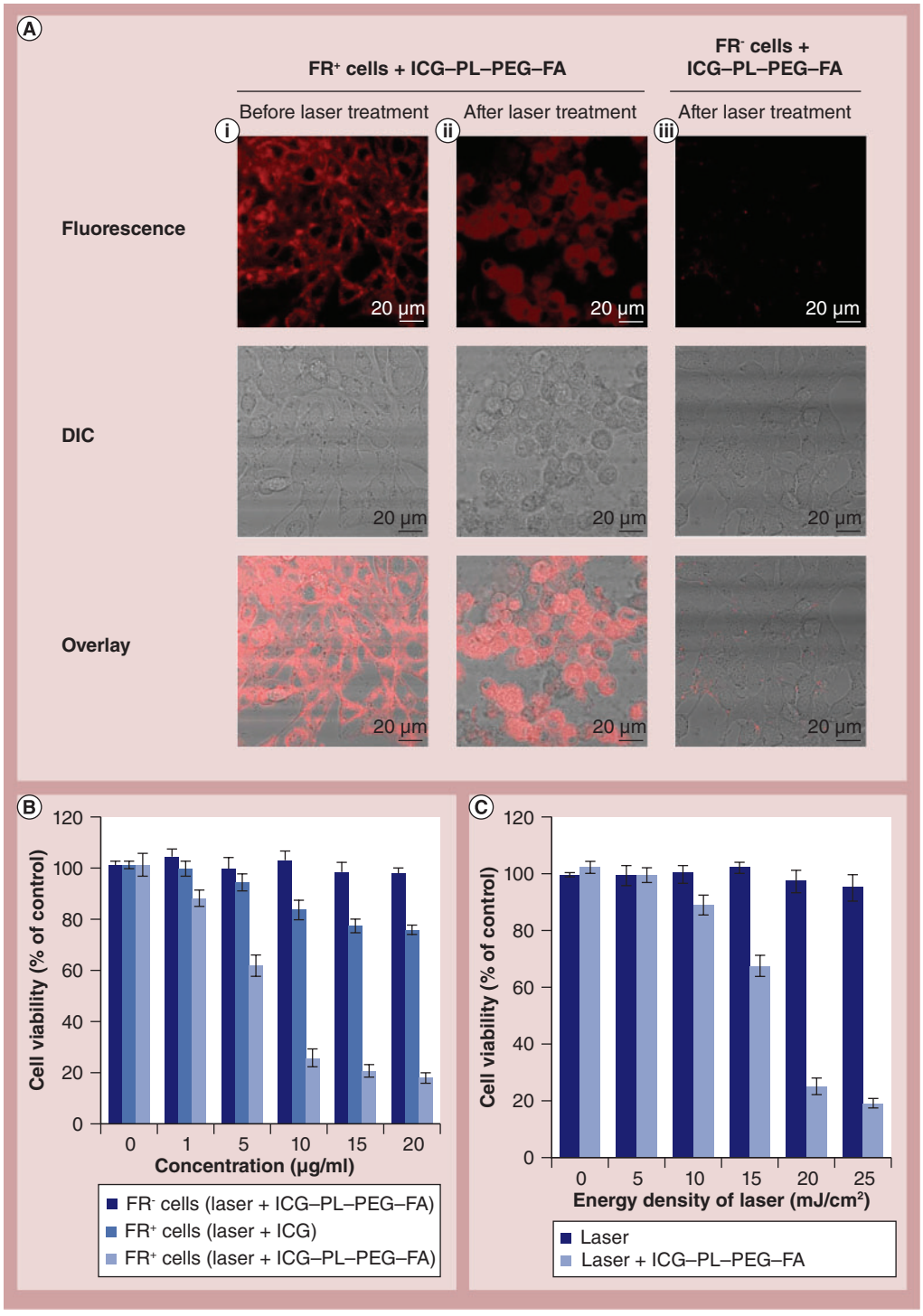

Figure 6. Targeted destruction of cancer cells by indocyanine green–phospholipid–polyethylene glycol–folic acid photoacoustic effect. (A) Confocal images of cancer cells under different treatments. FR^- cells remained unharmed under laser irradiation (20 mJ/cm^2; 20 s) without the probe. Extensive cell death was observed under laser irradiation after FR^+ cells were incubated with ICG–PL–PEG–FA. **(B)** Cell viability of FR^+ and FR^- cells after incubation with ICG–PL–PEG–FA or ICG (with different ICG concentrations) was assessed after near-infrared laser irradiation (20 mJ/cm^2; 20 s). Data are expressed as mean ± standard error of mean (n = 6). **(C)** Cell viability of FR^+ cells after incubation with the ICG–PL–PEG–FA NPs (containing 10 μg/ml ICG) was assessed after near-infrared laser irradiation with different irradiation energy densities for 20 s. Data are expressed as mean ± standard error of mean (n = 6).
DIC: Differential interference contrast measurement; FA: Folic acid; FR: Folate receptor; ICG: Indocyanine green; PL–PEG: Phospholipid–polyethylene glycol.

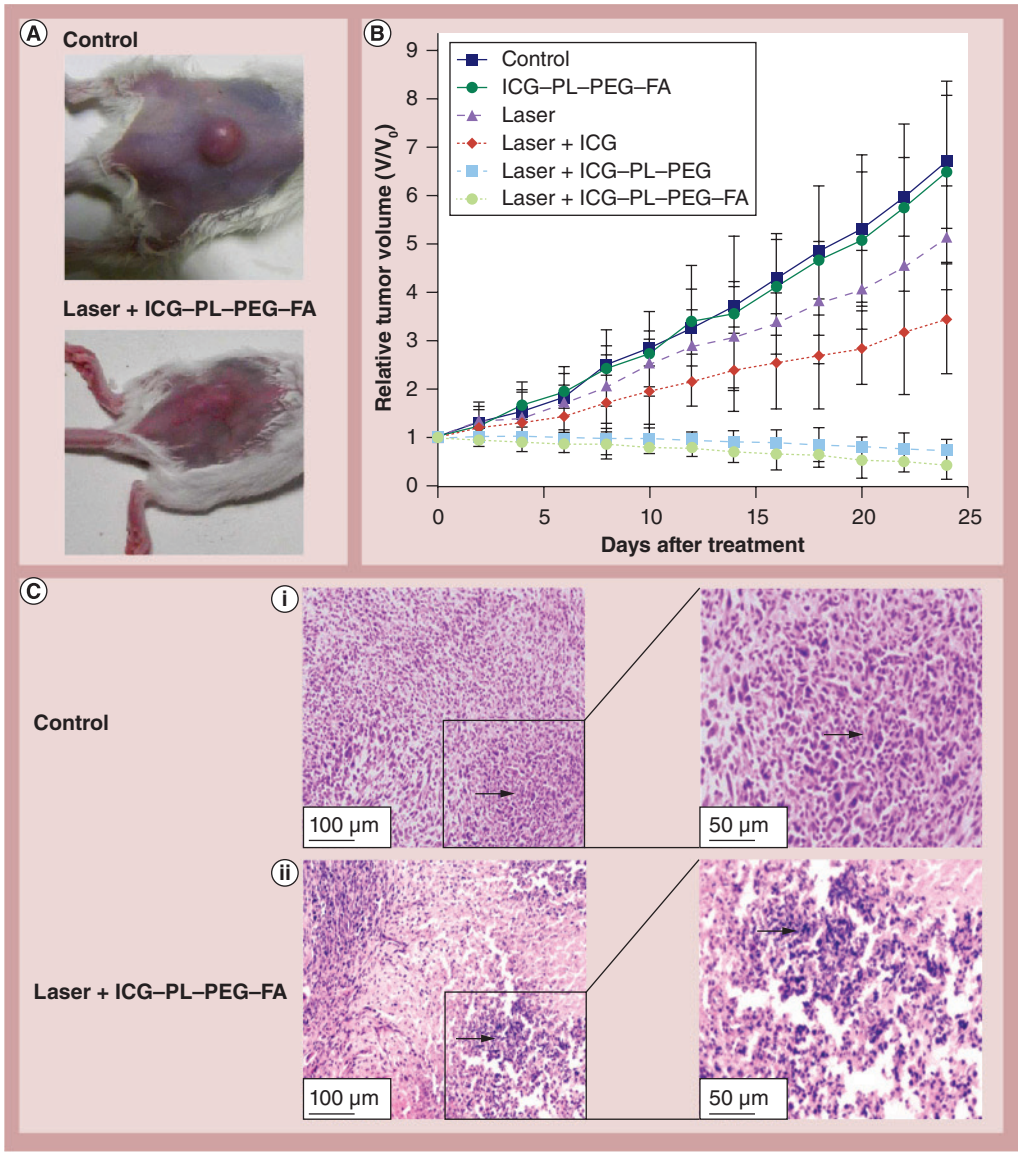

Figure 7. Photoacoustic treatment of tumor-bearing mice after intratumoral injection with indocyanine green, indocyanine green–phospholipid–polyethylene glycol or indocyanine green–phospholipid–polyethylene glycol–folic acid. (A) Representative photos of a laser + ICG–PL–PEG–FA-treated mouse and a control mouse. **(B)** Time-dependent tumor growth curves of EMT6 tumor (n = 5 per group) under different treatments. The relative tumor volumes were normalized to their initial sizes. **(C)** Images of hematoxylin and eosin-stained tumor sections harvested from a laser + ICG–PL–PEG–FA-treated mouse and a control mouse. Cancer cells were severely destroyed by the photoacoustic treatment (arrows).
FA: Folic acid; ICG: Indocyanine green; PL–PEG: Phospholipid–polyethylene glycol.

H+E-stained sections of major organs of the mice after 20 days with different treatments were examined; obvious organ damage was not observed (Figure 9C), indicating that ICG–PL–PEG NP-based photoacoustic therapy could be a safe cancer treatment technique.

During photoacoustic treatment, full-body thermographic images were captured using an infrared camera. The maximum surface temperature of the irradiated area was plotted as a function of the irradiation time. Figure 10 shows that the tumor experienced only a small temperature increase, which is entirely different from past photothermal techniques that heat the ICG–PL–PEG–FA in tumor tissue to high temperatures.

Discussion

The photoacoustic technique has a broad range of applications, including photoacoustic therapy, nondestructive biomedical imaging, chemical analysis and ecology [33–38]. The acoustic

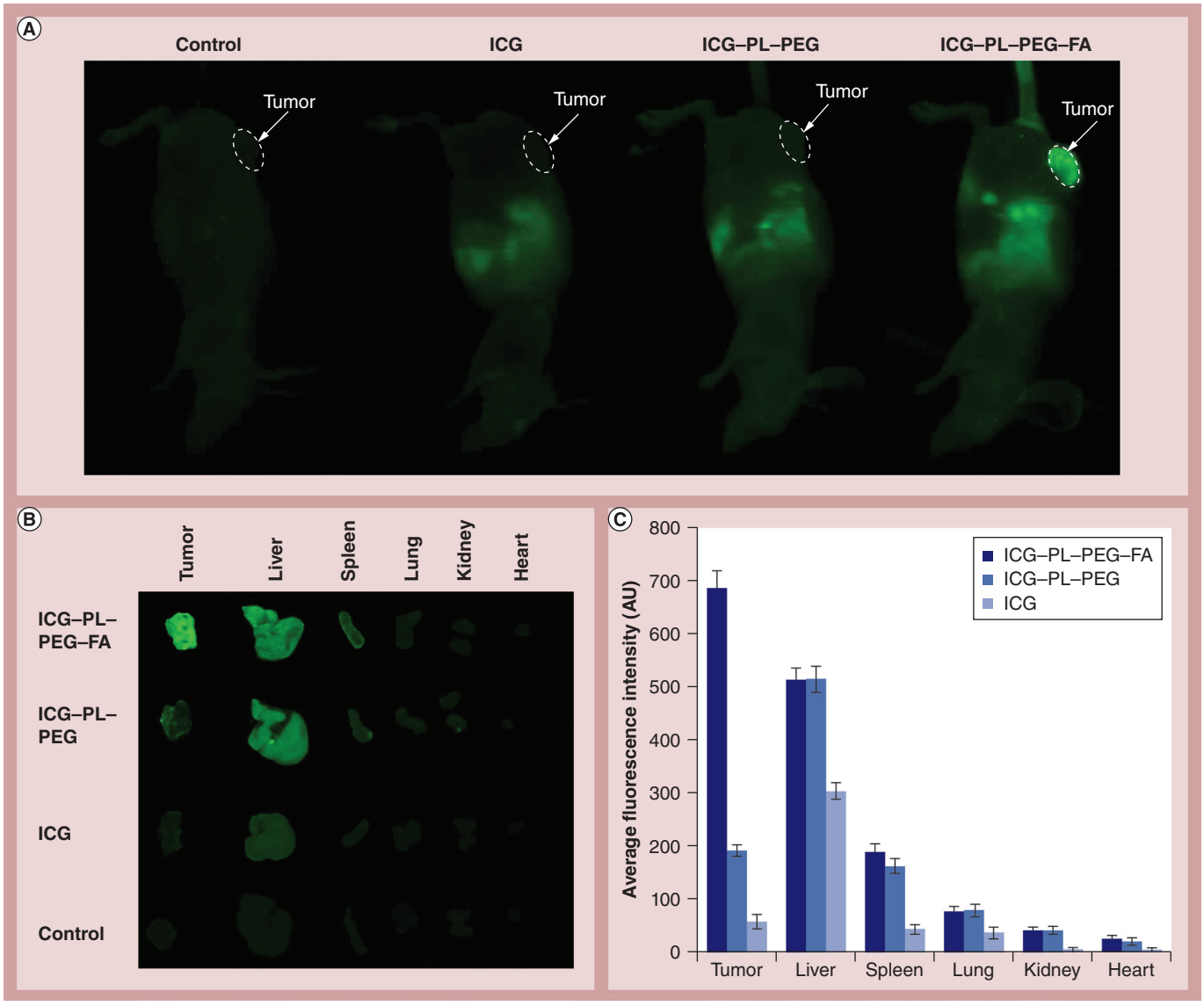

Figure 8. *In vivo* biodistribution analysis of indocyanine green, indocyanine green–phospholipid–polyethylene glycol and indocyanine green–phospholipid–polyethylene glycol–folic acid via tail vein injection in nude tumor-bearing mice. **(A)** The whole-body near-infrared fluorescent images of mice were taken at 6 h after intravenous injection. Detection was performed using the Odyssey® Infrared Imaging System (LI-COR Inc., NE, USA) through a 800-nm channel. ICG was mainly accumulated in the liver, while ICG–PL–PEG–FA had a high accumulation in both the tumor and liver. **(B)** Major organs of EMT6 tumor-bearing mice were collected for fluorescence imaging. Spectrally resolved *ex vivo* fluorescence images of different organs are displayed. **(C)** Semiquantitative biodistribution of ICG, ICG–PL–PEG and ICG–PL–PEG–FA in mice determined by the averaged fluorescence intensity of each organ (after subtraction by the fluorescence intensity of each organ before injection).
FA: Folic acid; ICG: Indocyanine green; PL–PEG: Phospholipid–polyethylene glycol.

waves are excited when pulsed light is absorbed by a target. There are several mechanisms of laser-generated acoustic waves [39–41]:

- In liquids, when the radiant power densities are below the vaporization threshold, acoustic waves are generated basically by the thermoelastic expansion. The absorption of light in a restricted volume induces thermal relaxation, resulting in the generation of acoustic waves;
- At high radiant intensities, when the absorbed energy exceeds the energy of evaporation, acoustic waves are generated by a recoil momentum arising upon liquid evaporation;
- When the laser radiation intensity exceeds the dielectric breakdown threshold, dielectric breakdown of the sample may occur.

Previous studies show that the photoacoustic pressure could reach 10^2–10^3 atm [13,14]. The amplitude of the photoacoustic wave depends

on both the optical absorption and the properties of the target. It is reported that NPs with strong optical absorption could significantly enhance the photoacoustic effect [42]. Such a strong photoacoustic effect could be used for the destruction of cancer cells.

As an FDA-approved NIR dye, ICG has been used for various therapeutic and diagnostic applications, such as imaging of retinal and choroidal vasculature since 1970 [43,44]. However, numerous disadvantageous physicochemical characteristics, such as poor aqueous stability, concentration-dependent aggregation and lack of target specificity, limit the application of ICG. Furthermore, ICG binds almost completely (98%) to plasma albumin, leading to its low vascular or tissue permeability [27,45]. ICG is taken up exclusively by the liver and secreted entirely into the bile after an intravenous injection. This behavior causes the rapid elimination of ICG from circulation, with an initial half-life of 3–4 min, followed by a slower half-life of approximately 1 h at lower concentrations. These properties lead to a low retention rate of ICG in tumor tissue [27,32].

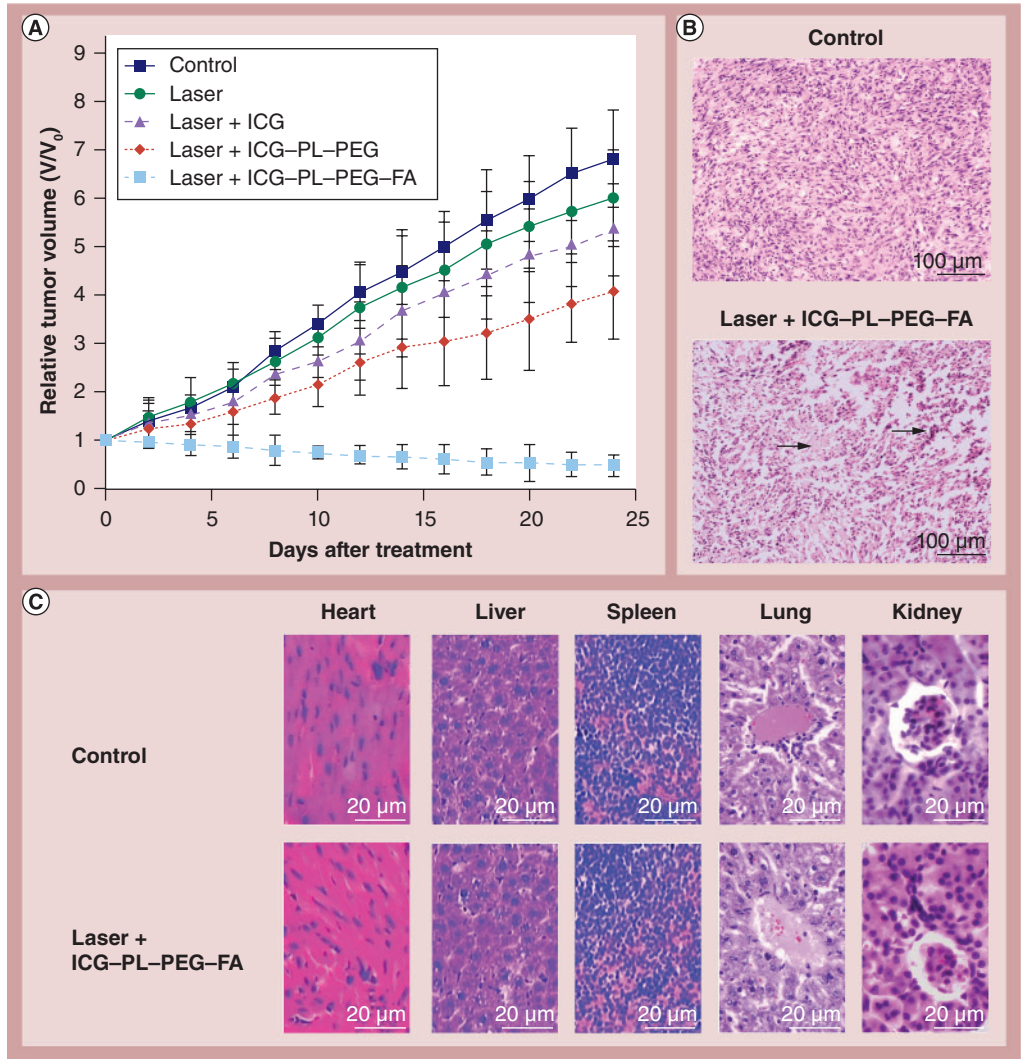

Figure 9. Photoacoustic treatment of tumor-bearing mice after intravenous injection with indocyanine green, indocyanine green–phospholipid–polyethylene glycol or indocyanine green–phospholipid–polyethylene glycol–folic acid. (A) Time-dependent tumor growth curves of EMT6 tumors (n = 5 per group) under different treatments. The relative tumor volumes were normalized to their initial sizes. **(B)** Images of hematoxylin and eosin-stained tumor sections harvested from a control mouse and a laser + ICG–PL–PEG–FA-treated mouse. Cancer cells were severely destroyed by the photoacoustic treatment (arrows). **(C)** Histological staining of the heart, liver, spleen, lung and kidney from a control mouse and a laser + ICG–PL–PEG–FA-treated mouse (20 days after treatment).
FA: Folic acid; ICG: Indocyanine green; PL–PEG: Phospholipid–polyethylene glycol.

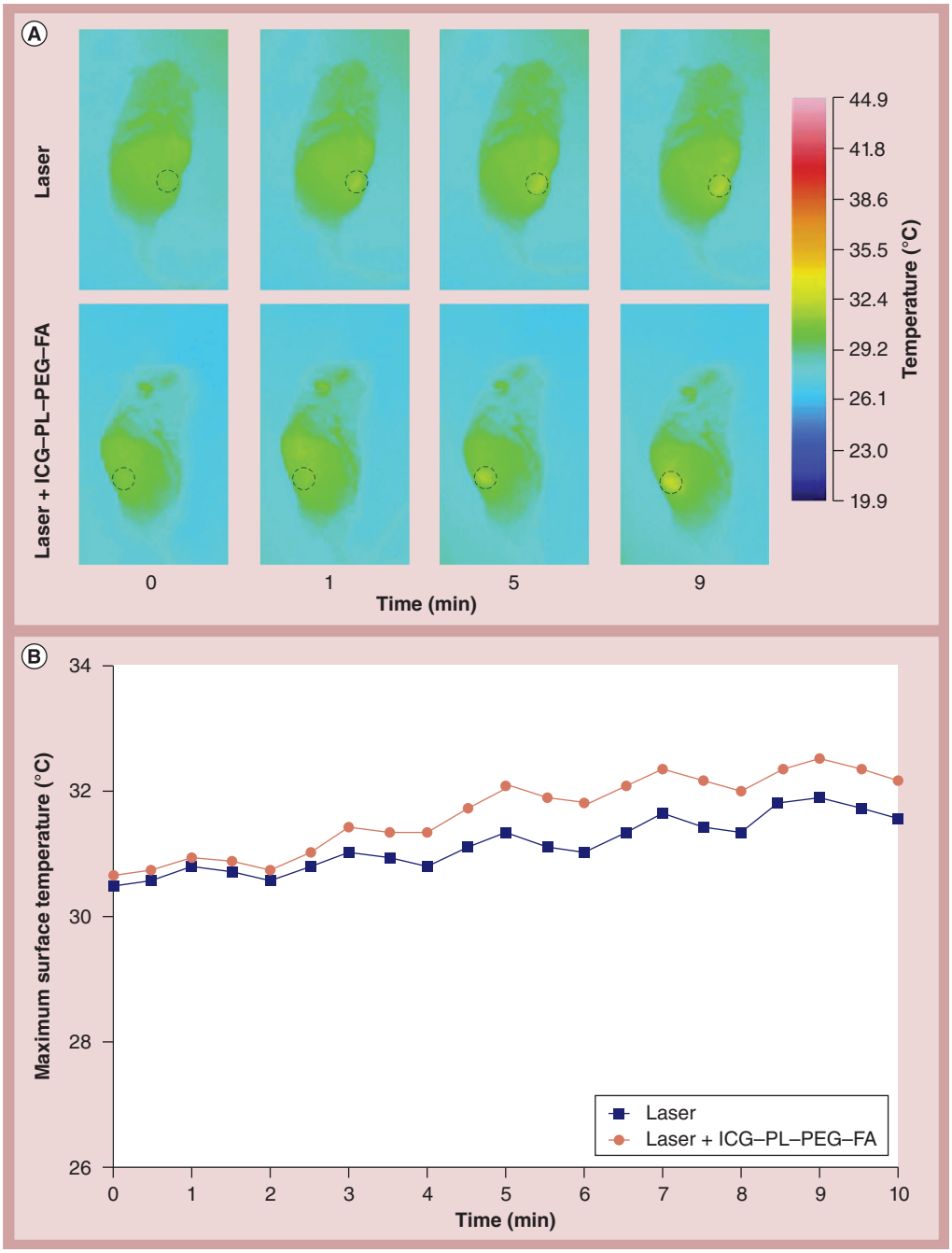

Figure 10. Monitoring of the changes in temperature on the surface of tumor tissue during laser treatment with or without indocyanine green–phospholipid–polyethylene glycol–folic acid intravenous injection. (A) Thermographic image of the group of laser + ICG–PL–PEG–FA injection versus laser treatment alone. **(B)** Temperature changes in the indicated region on the thermographic image. For color images please see online www.futuremedicine.com/doi/suppl/10.2217/NNM.12.145.
FA: Folic acid; ICG: Indocyanine green; PL–PEG: Phospholipid–polyethylene glycol.

To overcome these limitations, an ICG–PL–PEG NP consisting of ICG and PL–PEG is used. All of the components of the NPs are biocompatible and relatively nontoxic. PEG is also FDA approved for many applications such as biomedical imaging and therapy. The addition of PEG provides several advantages for the therapeutic application of ICG–PL–PEG:

- The hydrophilic PEG can render the NPs stable and compatible with biological media;
- PEG can reduce uptake by the reticulo–endothelial system in drug delivery;

- PEG can be used to provide the NPs with stealth properties for longer circulation times and to prolong serum half-lives *in vivo* [46–50];
- Amine groups at the free termini of PEG chains allow for conjugation of FA.

In addition, an ICG–PL–PEG suspension may be more efficient in producing a photoacoustic wave than ICG alone when irradiated by 808-nm laser pulses, based on the following reasons:

- With the same ICG concentration, ICG–PL–PEG has more efficient light absorption than ICG at 808 nm [32];
- The high concentration of ICG in the NPs [20];
- Encapsulation in a NP stabilizes ICG against an aqueous media and other destabilizing effects from the biological environment [20,23].

FA is a fascinating candidate for cancer cell targeting, because the FR is often overexpressed in many cancers, such as KB, HeLa cells and MCF7, while most normal tissues express low to negligible levels [51–55]. The targeting ICG–PL–PEG–FA NPs could promote not only their intracellular transport efficiency, but also specificity toward tumor cells. In this study, the ICG–PL–PEG–FA NPs bind to FR^+ cells at a much higher rate than to FR^- cells. *In vivo* tumor targeting and tumor accumulation of the ICG–PL–PEG–FA were also confirmed.

NPs can extravasate into the tumors through the enhanced permeability and retention effect [29]. However, most NPs mainly accumulate in the interstitial space of the tumor and can be easily cleared. The introduction of FA to the ICG–PL–PEG NPs could promote their specificity, penetration and distribution in the tumor. The results of this study demonstrate that ICG–PL–PEG–FA could effectively target tumor cells and increase NP accumulation in tumors.

While the authors' past ICG–PL–PEG NP studies have achieved a photothermal technique for cancer killing using long-time continuous laser irradiation, their current work demonstrated a new photoacoustic technique for cancer destruction using a pulsed laser [23]. When laser irradiation was used, the significant photoacoustic effect of ICG–PL–PEG NPs in the alginate–polylysine–alginate microcapsules was observed. The microcapsules were broken by the photoacoustic effect. The destruction caused by the photoacoustic effect is considered to be a kind of mechanical damage [7]. The photoacoustic destruction of treated FR^+ cells was shown to be highly selective. The destruction of FR^+ cells was due to the photoacoustic effect originating from the NPs. This is entirely different from past photothermal techniques that heat the ICG–PL–PEG solution to a high temperature and destroy cells through continuous laser irradiation at 2.75 W/cm^2 for 5 min [23].

When photoacoustic treatment was performed on mice, the laser and ICG–PL–PEG–FA treatment caused significant tumor suppression. Histological examinations of tumor tissues from each group further confirmed the successful destruction of tumor cells by the photoacoustic effect of ICG–PL–PEG–FA NPs. With H+E staining analysis, a high scathe level was observed in the laser- and ICG–PL–PEG–FA-treated tumors. These results show that the ICG–PL–PEG–FA NPs have a remarkable capability to enhance the photoacoustic destruction of tumor cells. Furthermore, H+E staining analysis demonstrated the absence of abnormal damage in the main organs that had high ICG–PL–PEG–FA uptake. In summary, the authors' work achieves effective NIR light-induced photoacoustic treatment in animal experiments using the targeting ICG–PL–PEG–FA NPs.

Conclusion

To the best of the authors' knowledge, this is the first report that ICG–PL–PEG–FA NPs can be used as cancer-targeting agents for the photoacoustic treatment of cancer. All of the components of ICG–PL–PEG–FA NPs are nontoxic. The destructive effect of ICG–PL–PEG–FA NPs on cancer cells can be considered mainly mechanical damage induced by the photoacoustic effect rather than the thermal damage caused by high temperature. The results show photoacoustic treatment with the targeting ICG–PL–PEG–FA NPs and laser pulses is an effective cancer therapy both *in vitro* and *in vivo*. In summary, laser and ICG–PL–PEG–FA treatment was proved to be a promising cancer-targeting photoacoustic treatment for cancer therapy.

Future perspective

With its outstanding properties, ICG–PL–PEG NPs conjugated with targeting agents can be used as an agent for photoacoustic imaging and selective photoacoustic therapy. The nonthermal mechanism of cell damage by the photoacoustic effect would not cause thermal side effects as in some surgical methods. In therapeutic applications, NP-based photoacoustic therapy may increase the efficacy and safety of cancer treatment, with the hope that one day it may offer patients a gentler yet effective alternative to current cancer therapies.

Financial & competing interests disclosure

This research was supported by the National Basic Research Program of China (2011CB910402; 2010CB732602), the Program for Changjiang Scholars and Innovative Research Team in University (IRT0829), and the National Natural Science Foundation of China (81127004; 11104087). The authors have no other relevant affiliations or financial involvement with any organization or entity with a financial interest in or financial conflict with the subject matter or materials discussed in the manuscript apart from those disclosed.

No writing assistance was utilized in the production of this manuscript.

Ethical conduct of research

The authors state that they have obtained appropriate institutional review board approval or have followed the principles outlined in the Declaration of Helsinki for all human or animal experimental investigations. In addition, for investigations involving human subjects, informed consent has been obtained from the participants involved.

Executive summary

Preparation of indocyanine green–phospholipid–polyethylene glycol–folic acid nanoparticles

- The indocyanine green (ICG)–phospholipid–polyethylene glycol (PL–PEG) nanoparticle (NP) is designed to utilize the noncovalent self-assembly chemistry between PL–PEG and ICG. It is an ideal light absorber for laser-mediated photoacoustic therapy.

***Cellular localization of the ICG–PL–PEG–folic acid NPs* in vitro**

- When conjugated with folic acid (FA), the ICG–PL–PEG–FA NPs were internalized by targeted cells via the ligand–receptor-mediated endocytosis pathway.

***Photoacoustic treatment of tumors* in vitro**

- Destruction of cancer cells was achieved *in vitro* when cells were incubated with the particles and irradiated with a near-infrared laser.

Tumor targeting of the ICG–PL–PEG–FA NPs

- ICG–PL–PEG–FA was shown to accumulate in tumors after intravenous injection.

***Photoacoustic treatment of tumors* in vivo**

- When photoacoustic treatment was performed on mice, the laser and ICG–PL–PEG–FA treatment caused significant tumor suppression.

Conclusion

- The authors' study has demonstrated the first use of ICG–PL–PEG–FA NPs for the targeted photoacoustic therapy of cancerous cells.
- The photoacoustic mechanism of cell detection and damage improves the selectivity and efficacy of cancer treatment. The results have the potential to be developed into a less toxic and more effective alternative to current cancer therapies.

References

Papers of special note have been highlighted as:
- ▪ of interest
- ▪▪ of considerable interest

1 Chatterjee DK, Yong Z. Upconverting nanoparticles as nanotransducers for photodynamic therapy in cancer cells. *Nanomedicine* 3(1), 73–82 (2008).

2 Zhou F, Wu S, Wu B, Chen WR, Xing D. Mitochondria-targeting single-walled carbon nanotubes for cancer photothermal therapy. *Small* 7(19), 2727–2735 (2011).

3 Hleb EY, Hafner JH, Myers JN *et al.* LANTCET: elimination of solid tumor cells with photothermal bubbles generated around clusters of gold nanoparticles. *Nanomedicine* 3(5), 647–667 (2008).

4 Jang B, Park J-Y, Tung C-H, Kim I-H, Choi Y. Gold nanorod-photosensitizer complex for near-infrared fluorescence imaging and photodynamic/photothermal therapy *in vivo*. *ACS Nano* 5(2), 1086–1094 (2011).

5 Zhou F, Xing D, Wu B, Wu S, Ou Z, Chen WR. New insights of transmembranal mechanism and subcellular localization of noncovalently modified single-walled carbon nanotubes. *Nano Lett.* 10(5), 1677–1681 (2010).

6 Choi WI, Kim J-Y, Kang C, Byeon CC, Kim YH, Tee G. Tumor regression *in vivo* by photothermal therapy based on gold-nanorod-loaded, functional nanocarriers. *ACS Nano* 5(3), 1995–2003 (2011).

7 Kang B, Yu D, Dai Y, Chang S, Chen D, Ding Y. Cancer-cell targeting and photoacoustic therapy using carbon nanotubes as "bomb" agents. *Small* 5(11), 1292–1301 (2009).

▪▪ **Reports a unique approach using the large photoacoustic effect of single-walled carbon nanotubes for the targeting and selective destruction of cancer cells.**

8 Chen J, Glaus C, Laforest R *et al.* Gold nanocages as photothermal transducers for cancer treatment. *Small* 6(7), 811–817 (2010).

9 Zhou F, Xing D, Ou Z, Wu B, Resasco DE, Chen WR. Cancer photothermal therapy in the near-infrared region by using single-walled carbon nanotubes. *J. Biomed. Opt.* 14(2), 021009 (2009).

10 Kang B, Dai Y, Chang S, Chen D. Explosion of single-walled carbon nanotubes in suspension induced by a large photoacoustic effect. *Carbon* 46(6), 978–981 (2008).

▪ **Reports a large photoacoustic effect of single-walled carbon nanotubes in suspension when the suspension is irradiated by a Q-switched pulsed laser.**

11 Kim K, Huang S-W, Ashkenazi S *et al.* Photoacoustic imaging of early inflammatory response using gold nanorods. *Appl. Phys. Lett.* 90(22), 223901 (2007).

12 Kim C, Favazza C, Wang LV. *In vivo* photoacoustic tomography of chemicals: high-resolution functional and molecular optical imaging at new depths. *Chem. Rev.* 110(5), 2756–2782 (2010).

▪ **An interesting review regarding the applications of the photoacoustic technique.**

13 Ostrovskaya GV. Efficiency of optical-to-acoustic energy conversion upon the interaction of a pulsed laser radiation with a liquid: I. Calculation of the efficiency upon acoustooptic interaction. *Technical Physics* 47(10), 1299–1305 (2002).

▪ **Reports on the efficiency of conversion of laser radiation energy to acoustic energy for the acousto–optic mechanism of interaction.**

14 Hoelen CGA, De Mul FFM. A new theoretical approach to photoacoustic signal generation. *J. Acoust. Soc. Am.* 106(2), 695–706 (1999).

15 Sharma R, Wendt JA, Rasmussen JC, Adams KE, Marshall MV, Sevick-Muraca EM. New horizons for imaging lymphatic function. *Ann. NY Acad. Sci.* 1131, 13–36 (2008).

16 Weissleder R. A clearer vision for *in vivo* imaging. *Nat. Biotechnol.* 19(4), 316–317 (2001).

17 Ogawa M, Kosaka N, Choyke PL, Kobayashi H. *In vivo* molecular imaging of cancer with a quenching near-infrared fluorescent probe using conjugates of monoclonal antibodies and indocyanine green. *Cancer Research* 69(4), 1268–1272 (2009).

18 Yu J, Javier D, Yaseen MA *et al.* Self-assembly synthesis, tumor cell targeting, and photothermal capabilities of antibody-coated indocyanine green nanocapsules. *J. Am. Chem. Soc.* 132(6), 1929–1938 (2010).

19 Kim C, Song KH, Gao F, Wang LV. Sentinel lymph nodes and lymphatic vessels: noninvasive dual-modality *in vivo* mapping by using indocyanine green in rats – volumetric spectroscopic photoacoustic imaging and planar fluorescence imaging. *Radiology* 255(2), 442–450 (2010).

20 Kim G, Huang SW, Day KC *et al.* Indocyanine-green-embedded PEBBLEs as a contrast agent for photoacoustic imaging. *J. Biomed. Opt.* 12(4), 044020 (2007).

21 Ku G, Wang LV. Deeply penetrating photoacoustic tomography in biological tissues enhanced with an optical contrast agent. *Opt. Lett.* 30(5), 507–509 (2005).

22 De La Zerda A, Liu Z, Bodapati S *et al.* Ultrahigh sensitivity carbon nanotube agents for photoacoustic molecular imaging in living mice. *Nano Lett.* 10(6), 2168–2172 (2010).

23 Zheng X, Xing D, Zhou F, Wu B, Chen WR. Indocyanine green-containing nanostructure as near infrared dual-functional targeting probes for optical imaging and photothermal therapy. *Mol. Pharm.* 8(2), 447–456 (2011).

▪▪ **A novel indocyanine green (ICG)-containing nanostructure was designed utilizing the noncovalent self-assembly chemistry between phospholipid–polyethylene glycol and ICG.**

24 Kim TH, Chen Y, Mount CW, Gombotz WR, Li X, Pun SH. Evaluation of temperature-sensitive, indocyanine green-encapsulating micelles for noninvasive near-infrared tumor imaging. *Pharm. Res.* 27(9), 1900–1913 (2010).

25 Kirchherr AK, Briel A, Ma Der K. Stabilization of indocyanine green by encapsulation within micellar systems. *Mol. Pharm.* 6(2), 480–491 (2009).

26 Rodriguez VB, Henry SM, Hoffman AS, Stayton PS, Li X, Pun SH. Encapsulation and stabilization of indocyanine green within poly(styrene-alt-maleic anhydride) block-poly(styrene) micelles for near-infrared imaging. *J. Biomed. Opt.* 13(1), 014025 (2008).

27 Benson RC, Kues HA. Fluorescence properties of indocyanine green as related to angiography. *Phys. Med. Biol.* 23(1), 159–163 (1978).

▪ **Reports the basic properties of ICG and shows how some clinical features related to basic properties also depend on the instrumentation used to perform ICG angiography.**

28 Brannon-Peppas L, Blanchette JO. Nanoparticle and targeted systems for cancer therapy. *Adv. Drug Deliv. Rev.* 56(11), 1649–1659 (2004).

29 Allen TM, Cullis PR. Drug delivery systems: entering the mainstream. *Science* 303(5665), 1818–1822 (2004).

30 Petros RA, Desimone JM. Strategies in the design of nanoparticles for therapeutic applications. *Nat. Rev. Drug Discov.* 9(8), 615–627 (2010).

31 Perrault SD, Walkey C, Jennings T, Fischer HC, Chan WC. Mediating tumor targeting efficiency of nanoparticles through design. *Nano Lett.* 9(5), 1909–1915 (2009).

32 Zheng X, Zhou F, Wu B, Chen WR, Xing D. Enhanced tumor treatment using biofunctional indocyanine green-containing nanostructure by intratumoral or intravenous injection. *Mol. Pharm.* 9(3), 514–522 (2012).

▪▪ **First time that an ICG-containing nanostructure has been used through systemic administration to achieve an efficient *in vivo* photothermal effect for cancer treatment.**

33 Yuan Y, Yang S, Xing D. Preclinical photoacoustic imaging endoscope based on acousto–optic coaxial system using ring transducer array. *Opt. Lett.* 35(13), 2266–2268 (2010).

34 Li L, Maslov K, Ku G, Wang LV. Three-dimensional combined photoacoustic and optical coherence microscopy for *in vivo* microcirculation studies. *Opt. Express* 17(19), 16450–16455 (2009).

35 Lao Y, Xing D, Yang S, Xiang L. Noninvasive photoacoustic imaging of the developing vasculature during early tumor growth. *Phys. Med. Biol.* 53(15), 4203–4212 (2008).

36 Ye F, Yang S, Xing D. Three-dimensional photoacoustic imaging system in line confocal mode for breast cancer detection. *Appl. Phys. Lett.* 97(21), 213702 (2010).

37 Yang S, Xing D, Lao Y *et al.* Noninvasive monitoring of traumatic brain injury and post-traumatic rehabilitation with laser-induced photoacoustic imaging. *Appl. Phys. Lett.* 90(24), 243902 (2007).

38 Guojia H, Sihua Y, Yi Y, Da X. Combining x-ray and photoacoustics for *in vivo* tumor imaging with gold nanorods. *Appl. Phys. Lett.* 99(12), 123701 (2011).

39 Bunkin FV, Komissatov VM. Optical excitation of sound waves. *Soviet Physics Acoustics* 19(3), 203–211 (1973).

40 Bunkin FV, Tribel'skii MI. Nonresonant interaction of high-power optical radiation with a liquid. *Soviet Physics – Uspekhi* 23(2), 105 (1980).

41 Lyamshev LM, Naugol'nykh KA. Optical generation of sound: nonlinear effects. *Soviet Physics - Acoustics* 27(5), 641–668 (1981).

42 Chen YS, Frey W, Aglyamov S, Emelianov S. Environment-dependent generation of photoacoustic waves from plasmonic nanoparticles. *Small* 8(1), 47–52 (2012).

43 Altinoglu EI, Russin TJ, Kaiser JM *et al.* Near-infrared emitting fluorophore-doped calcium phosphate nanoparticles for *in vivo* imaging of human breast cancer. *ACS Nano* 2(10), 2075–2084 (2008).

44 Flower RW. Evolution of indocyanine green-dye choroidal angiography. *Opt. Eng.* 34(3), 727–736 (1995).

45 Yoneya S, Saito T, Komatsu Y, Koyama I, Takahashi K, Duvoll-Young J. Binding properties of indocyanine green in human blood. *Invest. Ophthalmol. Vis. Sci.* 39(7), 1286–1290 (1998).

46 Sheng Y, Liu C, Yuan Y *et al.* Long-circulating polymeric nanoparticles bearing a combinatorial coating of PEG and water-soluble chitosan. *Biomaterials* 30(12), 2340–2348 (2009).

47 Davis ME, Zuckerman JE, Choi CHJ *et al.* Evidence of RNAi in humans from systemically administered siRNA via targeted nanoparticles. *Nature* 464(7291), 1067–1070 (2010).

48 Jokerst JV, Lobovkina T, Zare RN, Gambhir SS. Nanoparticle PEGylation for imaging and therapy. *Nanomedicine* 6(4), 715–728 (2011).

49 Nel AE, Maedler L, Velegol D *et al.* Understanding biophysicochemical interactions at the nano–bio interface. *Nat. Mat.* 8(7), 543–557 (2009).

50 Sun C, Veiseh O, Gunn J *et al. In vivo* MRI detection of gliomas by chlorotoxin-conjugated superparamagnetic nanoprobes. *Small* 4(3), 372–379 (2008).

51 Zheng C, Zheng M, Gong P *et al.* Indocyanine green-loaded biodegradable tumor targeting nanoprobes for *in vitro* and *in vivo* imaging. *Biomaterials* 33(22), 5603–5609 (2012).

▪ **Folic acid–ICG–poly(D,L-lactide-*co*-glycolide)–lipid nanoparticles were specifically targeted to the tumor, and its circulation time was much longer than free ICG.**

52 Gabizon A, Tzemach D, Gorin J *et al.* Improved therapeutic activity of folate-targeted liposomal doxorubicin in folate receptor-expressing tumor models. *Cancer Chemother. Pharmacol.* 66(1), 43–52 (2010).

53 Parker N, Turk MJ, Westrick E, Lewis JD, Low PS, Leamon CP. Folate receptor expression in carcinomas and normal tissues determined by a quantitative radioligand binding assay. *Anal. Biochem.* 338(2), 284–293 (2005).

54 Kaaki K, Herve-Aubert K, Chiper M *et al.* Magnetic nanocarriers of doxorubicin coated with poly(ethylene glycol) and folic acid: relation between coating structure, surface properties, colloidal stability, and cancer cell targeting. *Langmuir* 28(2), 1496–1505 (2012).

55 Choi SJ, Choy JH. Layered double hydroxide nanoparticles as target-specific delivery carriers: uptake mechanism and toxicity. *Nanomedicine* 6(5), 803–814 (2011).